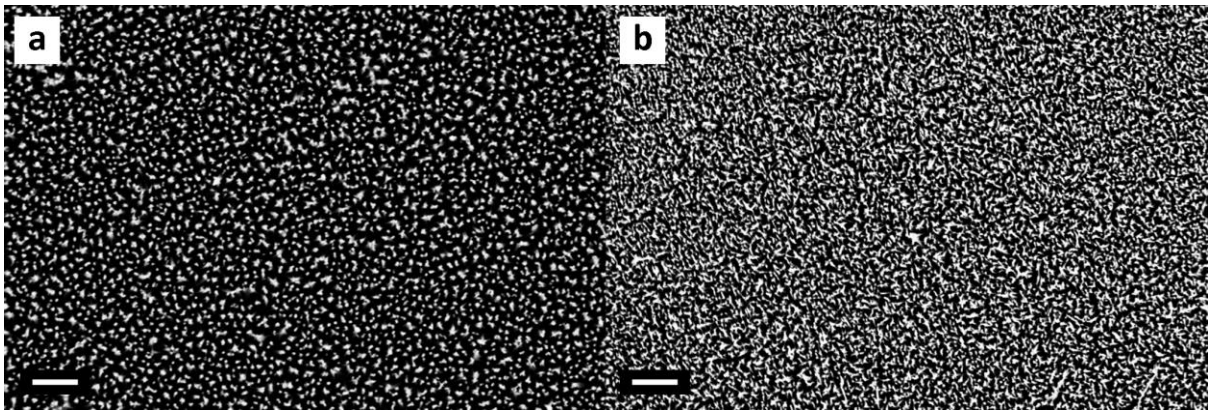

Supplementary Figure S1 | Black silicon and dragonfly wing nanotopography. Representative low-magnification scanning electron micrographs of **a)** Black silicon (bSi) and **b)** *Diplacodes bipunctata* dragonfly wing surfaces. Both images were recorded at 15000× magnification, and are representative of images taken from various regions of their respective samples. Scale bars = 1 μm.

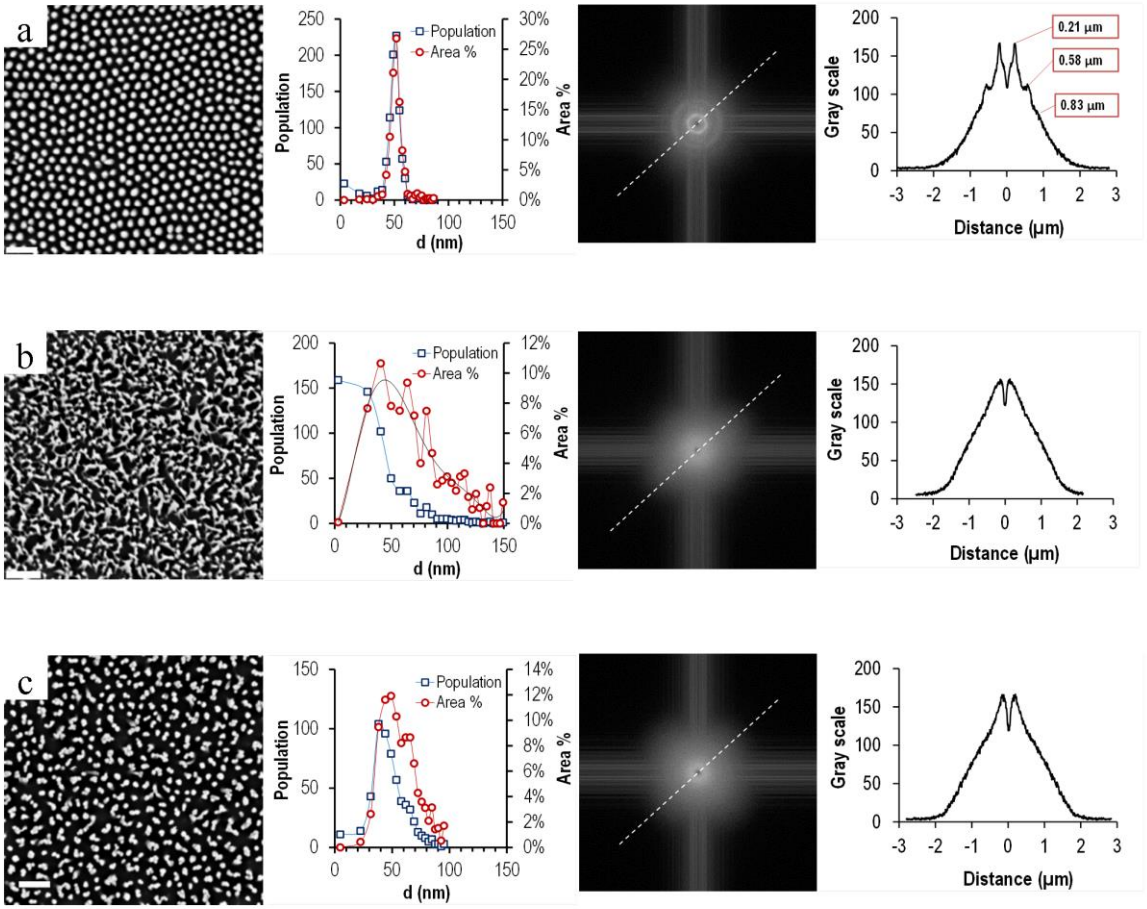

Supplementary Figure S2 | Topographical analysis of bactericidal surfaces. Image analysis of upper plane topology of three bactericidal surfaces **a)** cicada wing, **b)** dragonfly wing, and **c)** bSi comprising original vertical SEM images band pass filtered to delineate the boundary of pillar clusters in the uppermost plane, providing initial bacterial contact together with their respective Fourier transform images, particle characteristics and spatial arrangement. Radial distributions of FT images were taken at 45° for clarity. Scale bars = 500 nm.

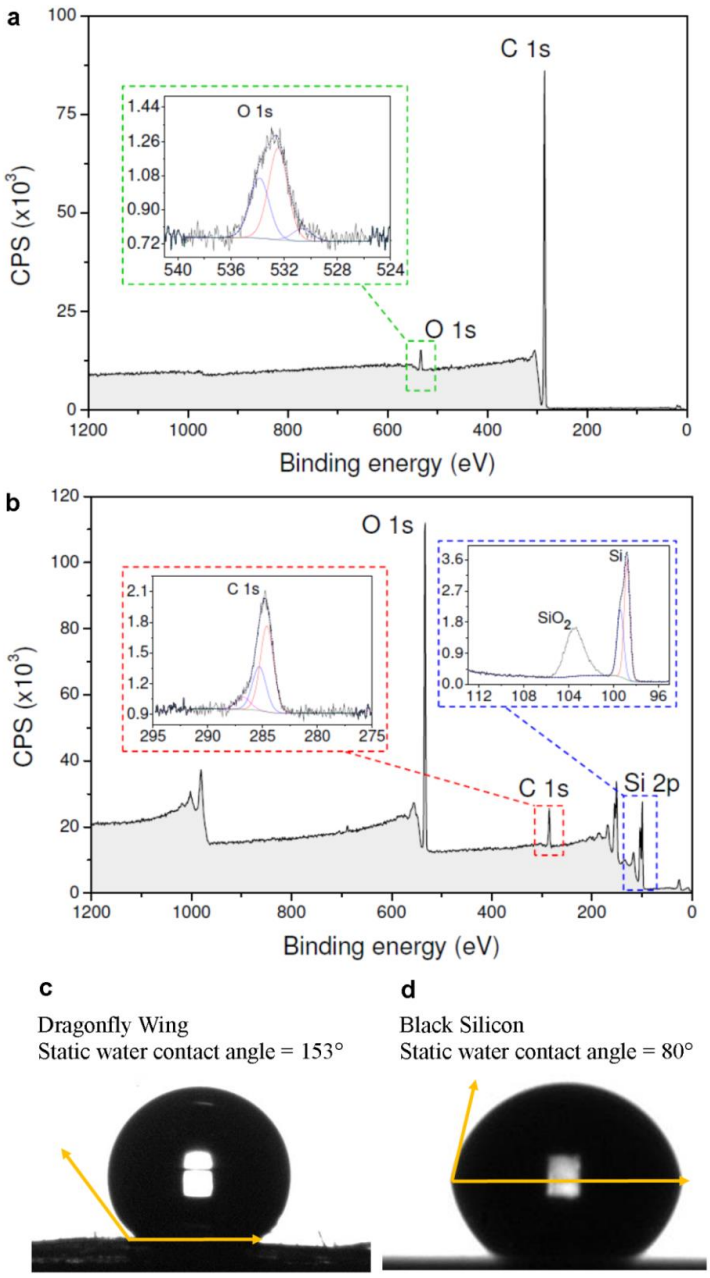

Supplementary Figure S3 | Chemical composition and surface wettability. X-ray photoelectron spectral information with survey scans conducted in the range of 0 to 1400 eV to determine elemental composition on the top layer of **a)** dragonfly wings and **b)** bSi surface. High-resolution scans (inset) were then performed in approximately 20 eV intervals across the O 1s and C 1s peaks. Static contact angle measurements **c)** dragonfly wings and **d)** bSi surface indicate that the wing surfaces are superhydrophobic whereas the bSi surfaces were relatively lower in hydrophobicity.

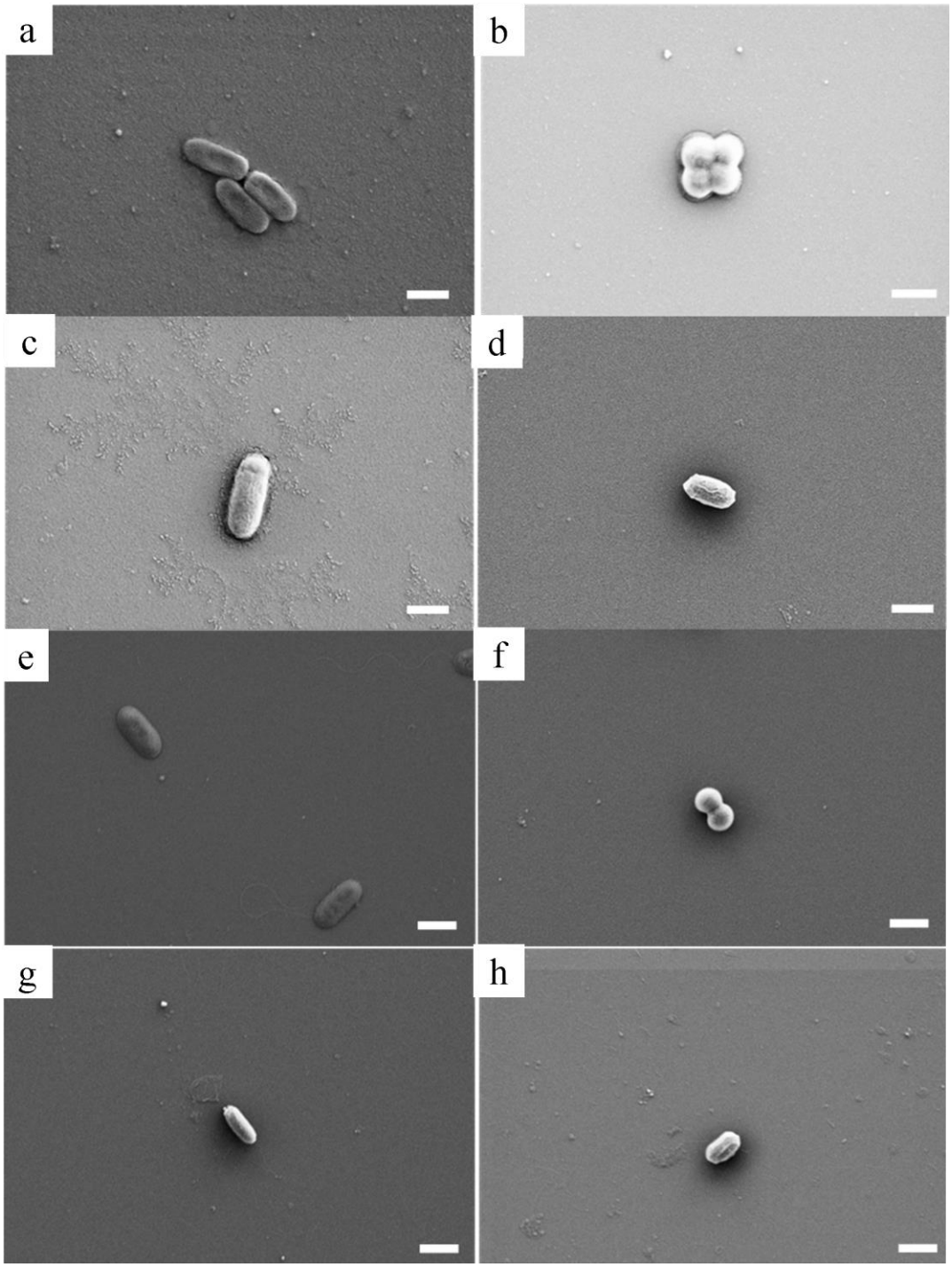

Supplementary Figure S4 | Bacterial morphology on control surfaces. Scanning electron microscopy images exhibiting cellular morphology of (**a, e**) *Pseudomonas aeruginosa*, (**b, f**) *Staphylococcus aureus*, (**c, g**) *Bacillus subtilis* vegetative cells and (**d, h**) *B. subtilis* spores on glass (**a-d**) and smooth silicon (**e-h**) control surfaces. Scale bars = 1 µm.

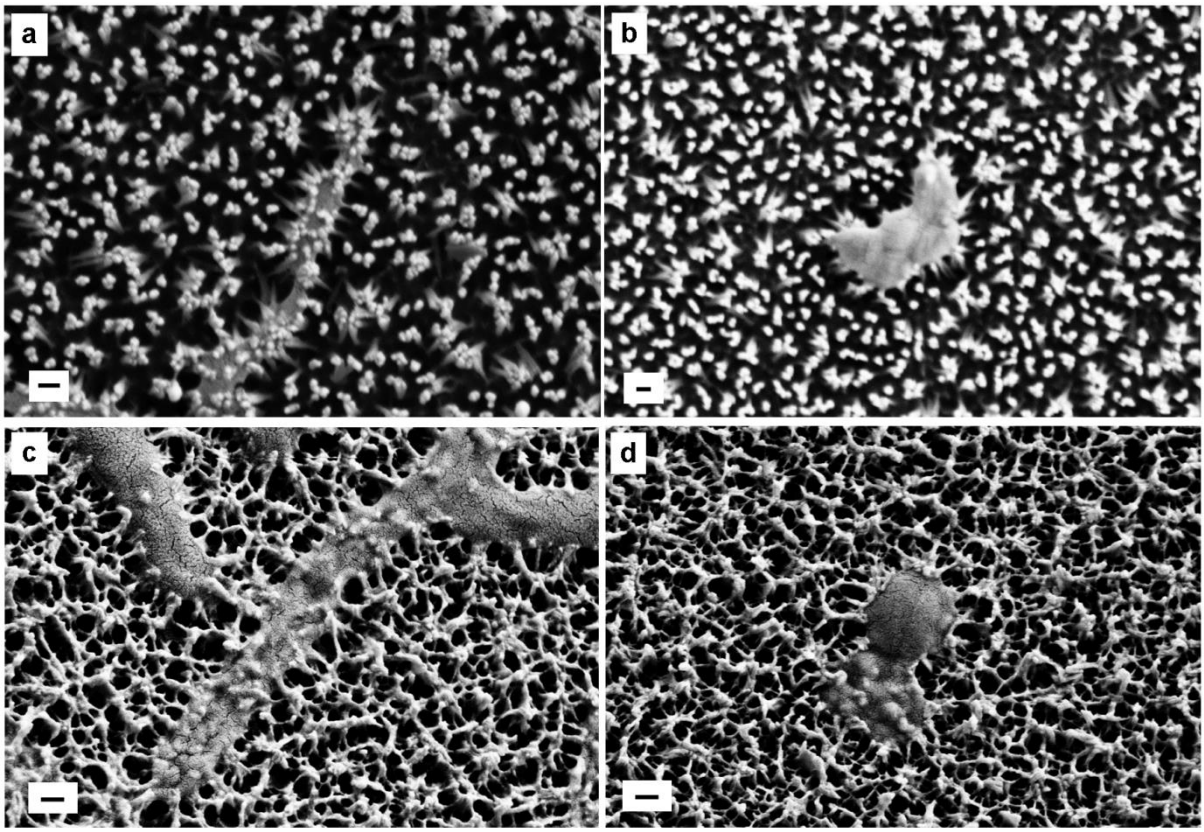

Supplementary Figure S5 | Bacterial morphology on gold coated black silicon and dragonfly wings. Bactericidal activity of gold-coated bSi and *D. bipunctata* dragonfly wings showing the pillar penetration of the cells causing them to be engulfed into the surface. Both the bSi (**a**, **b**) and dragonfly wings (**c**, **d**) maintained their bactericidal activity against *Pseudomonas aeruginosa* (**a**, **c**) and *Staphylococcus aureus* (**b**, **d**). The continued activity when Au coated together with the wide range of surface hydrophobicities between dragonfly wing and bSi surfaces confirms physical mechano-interactions as the primary mechanism of bactericidal activity rather the surface chemical interactions. Scale bars = 200 nm.

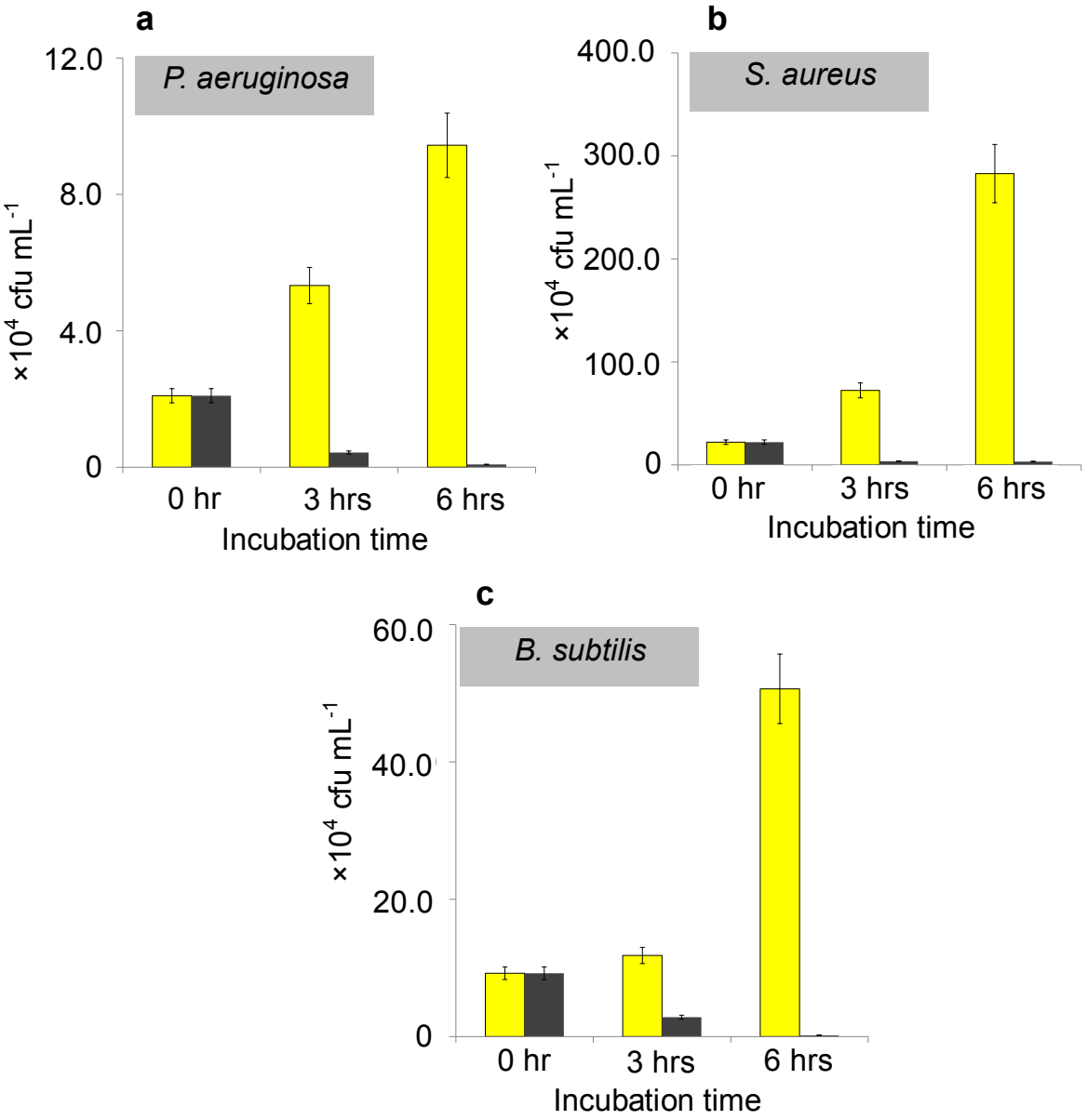

Supplementary Figure S6 | Bactericidal activities of black silicon surfaces in nutrient rich environment at 37 °C. Viable cells remaining in suspension after 3 h and 6 h when incubated with bSi (grey columns) and control suspensions (yellow columns) were recovered by direct plating on the nutrient agar plates.

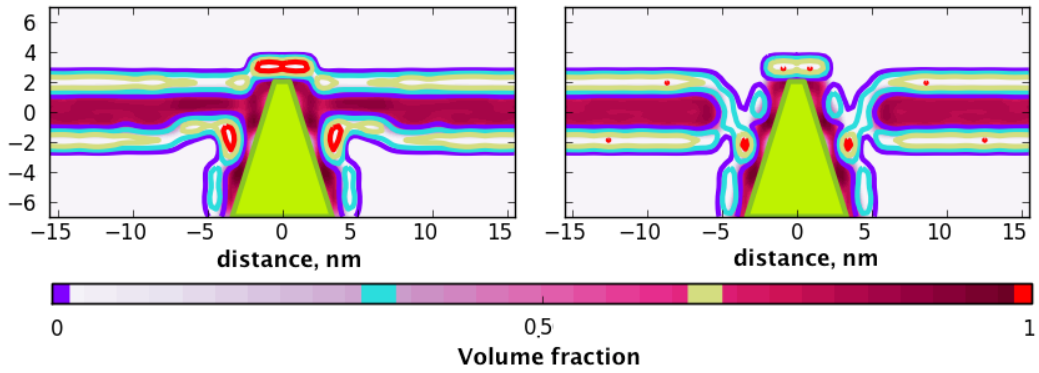

Supplementary Figure S7 | Membrane interaction model. Suggested mechanism of formation of toroidal pore in the lipid bilayer due to interactions with hydrophobic tip of bSi nanoprotrusions (green cone) obtained by SCMF theory[7]. The tails of phospholipids are coded with filled areas; the lipid heads are coded with empty areas. Colour intensity designates the volume fraction from 0 to 1. Strong attraction of phospholipid tails to the surface of the tip (interaction energy -10 kT per tail bead[40]) leads to spontaneous reorientation of lipids inside the bilayer and formation of a toroidal pore.

Supplementary Methods

Structural analysis of black silicon and dragonfly wing surfaces

Image analysis of the uppermost plane of the surface topology, which provides the site for the initial contact with bacteria cells, was carried out on band pass filtered SEM images of three bactericidal surfaces (a) cicada wing, (b) dragonfly wing, and (c) black silicon (bSi) (Supplementary Fig. S1 and Supplementary Fig. S2a-c). In this upper plane, these disordered pillar clusters were analysed for size, shape and spatial distribution using the filtered SEM images and their Fourier transforms to allow surface contact topography to be obtained. Clearly, in terms of bacterial contact, bSi represents a biomimetic analogue of the more disordered dragonfly surface, whilst the cicada wing exhibits a 2-D array of individual pillars.

Chemical analysis of black silicon and dragonfly wing surfaces

Insect wings exhibit a complex chemical composition, which is predominately attributable to various hydrophobic lipids and waxes[38,39]. X -ray photoelectron spectroscopy (XPS) survey spectra (Supplementary Fig. S3a) demonstrated that *D. bipunctata* wings surfaces were composed of 97.5 at.% C and 2.5 at.%. O, consistent with a surface that is covered by hydrophobic lipid molecules with long carbon-chain backbones and fatty acid molecules that are associated with a relatively small portion of the surface lipids. In contrast, the XPS spectra of the bSi revealed the presence of primarily only two elements, O and Si, due to the presence of amorphous Si (Supplementary Fig. S3b).

Bacterial morphologies and attachment on non-modified and nanostructured surfaces

The surface chemistry and structure of dragonfly wings rendered them superhydrophobic, whilst bSi was significantly less hydrophobic (Supplementary Fig. S3d), largely due to surface oxidation that occurs during its fabrication. The morphology of bacterial cells and spores on the nanostructured dragonfly and bSi surfaces (Fig. 1a-b) can be compared to their undeformed state on the planar glass and silicon control surfaces as shown in Supplementary Fig. S4. SEM images of gold-coated bSi and dragonfly wing surfaces show that the *Pseudomonas aeruginosa* (Supplementary Fig. S5a and S5c) and *Staphylococcus aureus* (Supplementary Fig. S5b and S5d) undergo cell deformation, engulfment and pillar penetration under the stresses imposed by pillar clusters, showing that the deformation is independent of the surface chemical composition and consistent with the independence of bactericidal activity from pillar wetting characteristics as shown by their micro-contact angles.

Bactericidal activities of bSi against pathogenic bacteria in nutrient-rich environments

P. aeruginosa, S. aureus and *B. subtilis* cells and spores were suspended in 5 mL of Difco nutrient broth (BD Diagnostic System, Sparks, MD, USA) and adjusted to OD_{600} = 0.1. The concentration of re-suspended cells was adjusted to corresponding infective doses which were 2.1×10^4 viable cells mL^{-1} for *P. aeruginosa*, 2.2×10^5 viable cells mL^{-1} for *S. aureus* and 9.2×10^5 viable cells mL^{-1} for *B. subtilis*[23-26]. In order to cover a surface of 1 cm^2, a drop of 10 µL of cell suspensions was placed on the bSi surfaces. Two independent experiments were carried out in triplicate for each time interval (0, 3 and 6 hours). All samples were incubated at 37 °C. After incubation with the surfaces, the respective cell suspensions were collected (10 µL), serially diluted 1:10, and each dilution spread on two nutrient agar plates. Resulting colonies were then counted using standard plate counts techniques[37], and the

number of colony forming units per mL calculated. The number of colony forming units was assumed to be equivalent to the number of viable cells in suspension[37].

The results indicated that after 6 hours the number of viable cells in the original suspensions increased exponentially approximately 4 – 12 times, depending on the strain (Supplementary Fig. S6). In contrast, the number of viable cells in the samples incubated on the bSi surfaces reduced significantly after 3 hours and were eliminated after 6 hours.

Theoretical modelling of the bactericidal mechanism of black silicon surfaces

The high bactericidal efficiency of bSi and dragonfly wings with respect to cicada wings[9] can be attributed to the nano-patterns on their surfaces. The bSi surfaces have long (250 - 500 nm) and thin (10 - 20 nm) spikes with sharp tips (Fig. 1a, Supplementary Fig. S1), in comparison to the thick pillars with round tips (60 nm) present on cicada wings[7]. The nanometer-scale sharp tips of bSi are comparable, in order of magnitude, to the thickness of the cell membranes, and thus can pierce the wall. In contrast, cicada wings possess blunt and round pillars with dimensions much larger than the thickness of the membrane. In the latter case, the membrane can adsorb onto the pillar surface and ruptures due to stretching of the membrane between the pillars[9], which may limit the efficiency with respect to direct piercing of the membrane. To quantify this mechanism, which is active in the case of bSi and dragonfly wings, we have used the Single Chain Mean Field (SCMF) theory of lipid bilayers, which can adequately describe the equilibrium and mechanical properties of lipid bilayers and provide microscopic information on the interaction and piercing of bilayers by nano-objects[40]. By constructing the interacting object in form of a cone with the dimensions of the tip of bSi taken from Fig 1a, and using a 3-beads model for lipid molecules[40], we have tested the interaction of the cone with the lipid bilayer as a function of the distance of the tip from the center of the bilayer (Supplementary Fig. S7). The number of lipids in a simulation box of

30 nm was kept constant at approximately 3000 which corresponds to an unperturbed equilibrium lipid bilayer with the area per lipid approximately 60 $Å^2$. Periodic boundary conditions model the periodic pattern of identical spikes in horizontal dimensions. The interactions of the lipids with the tip are chosen to be -10 kT, and the resulting structure was consistent with the results obtained with other geometries[41]. At small insertions, the cone attracts the lipids without changing the topology of the bilayer. However, at some intermediate insertions there is an abrupt change of the bilayer structure associated with formation of a pore around the tip (Supplementary Fig. S7). The tails of lipids are attracted to the surface of the tip[42], this in turn, induces the reorientation of the lipids heads pointing outward from the surface of the cone and thus, formation of a toroidal pore. At the transition point, shown in Supplementary Fig. S7, two solutions corresponding to topologies with and without pore coexist, thus indicating that the transition is similar to first order transitions and the pore is formed spontaneously. This mechanism does not require deep insertions of the membrane into the pattern as it was suggested for cicada wings surfaces[9] and, as can be seen from Supplementary Fig. S7, the bacterial cells are ruptured by bSi pattern in contact with the tips of the spikes.

Thus, the result of these physical interaction forces and their respective stresses on the whole cell bodies leads to significant deformation and cell death over the broad suite of bacteria types, and which may be categorized as a mechano-responsive approach compared to the established surface chemical approaches to bactericidal materials.

Supplementary References

38. Vincent, J. F. V. Arthropod cuticle: a natural composite shell system. *Compos. Part A Appl. Sci. Manuf.* **33**, 1311-1315 (2002).

39. Vincent, J. F. V. & Wegst, U. G. K. Design and mechanical properties of insect cuticle. *Arthropod Struct. Dev.* **33**, 187-199 (2004).

40. Pogodin, S. & Baulin, V. A. Can a carbon nanotube pierce through a phospholipid bilayer? *ACS Nano* **4**, 5293-5300 (2010).

41. Pogodin, S. & Baulin, V. A. Equilibrium insertion of nanoscale objects into phospholipid bilayers. *Curr. Nanosci.* **7**, 721-726 (2011).

42. Savarala, S., Ahmed, S., Ilies, M. A. & Wunder, S. L. Formation and colloidal stability of DMPC supported lipid bilayers on SiO_2 nanobeads. *Langmuir* **26**, 12081-12088 (2010).